Pressure drop reconstruction in the aqueduct of sylvius from MRI acquisitions

Gérald Bardan, Franck Plouraboué, Mokhtar Zagzoule, Olivier Balédent

Pressure drop reconstruction in the aqueduct of sylvius from MRI acquisitions

G. Bardan*, F. Plouraboue, M. Zagzoule and O. Baledent

IMFT, UMR 5502, 31400 Toulouse, France

Keywords: Aqueduct of Sylvius; Cerebro-spinal liquid; Pulsatile flows

1. Introduction

From measurement of the oscillating flux of the cerebro-spinal liquid (CSL) in the aqueduct of Sylvius, we elaborate a patient-based methodology for pressure evaluation. High-resolution anatomical MRI first permits a precise three-dimensional anatomical digitalyzed reconstruction of the Sylvius's aqueduct shape. Cine phase-contrast MRI is now an invaluable tool for pathologies investigations (Tain and Alperin 2009) for the evaluation of blood flow in then brain vessels as well as inside the CSL flow inside the brain cavities. It permits the evaluation of the CSL pulsatile flux inside the aqueduct. Produced mainly in the lateral and third ventricules, CSL flows along the aqueduct of Sylvius to reach the fourth ventricle, then passes into the Sub-Arachnoid Spaces (SAS) and is absorbed mainly into sagittal sinus blood. Under normal circumstances CSL oscillates in and out ventricular cavities with a net outward flow Q_S equals to the CSL physiological production rate. The aqueduct, is a slighly curved pipe with a variable elliptic section. It is the smallest cavity between Lateral Ventricules and SAS. This is where most of the viscous dissipation and thus where most of the pressure drop occurs (Sweetman et al. 2011). The aqueduct influence on the pressure distribution inside the brain's cavities thus deserves special attention, especially in the context of stenotic conditions (Fin and Grebe 2003). We show that a slighly curved, low Dyne number and small reduced Reynolds approximation for the CSL oscillation inside the aqueduct of Sylvius is a fair description. It permits to develop a very fast estimate of the pressure drop, shear and hydraulic admittance.

2. Methods

From patient-based anatomical reconstructed of the aqueduct, we develop a very fast approximated numerical flow computation. This computation leads to a flux which is also consistently compared with previous analytical predictions. Our approach includes the main contributions of inertia effects coming from pulsatile flows as well as curvature influence associated with the aqueduct bending. Integrating the flow along the aqueduct longitudinal centerline permits the evaluation of the total dynamic hydraulic admittances of the aqueduct. Such equivalent frequency-dependent electric impedance descriptions are, to our knowledge, the first explicit evaluation provided in an healthy population. The anatomical orientation of the aqueduct is sagital and mostly vertical. Thus, it is possible to provide its reliable three-dimensional digitalized reconstruction from analyzing each successive horizontal section of the aqueduct. In each horizontal section, we first extract the elliptical contour that best fits the gray level anatomical image of the aqueduct. For each ellipse, following the curvilinear lengths along the centreline, the center, the major radius a(s) and minor radius b(s) are extracted. From the evaluation of ellipse's center in each successive horizontal section, the aqueduct centreline is reconstructed. Hence, it is easy to evaluate the main radius of curvature of the resulting planar centreline curve. Using a quadratic minimization among the discrete set of n points of the centrelines, it is possible to extract the main radius of curvature R_c of the aqueduct centreline which quantifies its bending in the sagittal plane as well as the curvilinear length L of the centerline.

3. Results and Discussion

We use an asymptotic approach for the flow evaluation. Since the aqueduct is slightly bended, the curvilinear length s is non-dimensionalyzed by the radius of curvature R_c, $s* = R_c\, s$, whereas the radial coordinate $r^* = \bar{a}r$, is non-dimensionalyzed by the typical transverse length $\bar{a}$ which is the average of the aqueduct elliptical contour major axis. The forcing pulsation is used to define dimensionless time $t* = t/\omega$, where the typical longitudinal velocity provides the scaling for the longitunal velocity component $u* = Uu$. A viscous pressure is used for the pressure non-dimensionalization since we consider moderate reduced Reynolds numbers so that $p* = (\mu\, U\, L/\bar{a}^2)p$.

Un-stationary viscous dominated flows are associated with dimensionless numbers called Womersley number

$\alpha^2 = \omega \bar{a}^2/\nu$. The dimensionless flux is defined by $Q* = U\bar{a}^2 Q$ where $Q*$ is given by MRI acquisitions. The longitudinalvelocity component is linked with local longitudinal pressure gradient $\partial p/\partial s$ by

$$\nabla^2 u - \alpha^2 \frac{\partial u}{\partial t} = -\frac{\partial p}{\partial s}$$

where ∇^2 is the Laplacian operator in the plane locally orthogonal to the centreline at curvilinear distance s, to be solved using boundary condition $u = 0$. The local pressure gradient is decomposed into a stationary $K_s(s)$ and unstationary $K_u(s)$ components: $\partial p/\partial s = K_s + K_u e^{it}$. The experimental flux is decomposed into discrete Fourier modes from a signal having 32 points per cardiac cycle. The zeroth's mode corresponds to the stationary flux Q_s. From the $f^k = 2\pi/\omega^k$ frequency we compute the sequence of Womersley numbers α^k for which the admittance Y^k is evaluated for a flux amplitude Q_u^k with $Q_u^k = Y^k \Delta P^k$. ΔP^k is the pressure difference obtained between the two extremity of the aqueduct of lenght L for a flux amplitude Q_u^k. The real and imaginary components of $Y^k = C^k + iS^k$ are called conductance and susceptance respectively. Figure 1 illustrates the result for the admittance real (C) and imaginary (S) components versus any chosen Womersley number α. The Fourier decomposition of the patient's temporal flux variations are then selecting discrete values α^k for which a discrete admittance reflects the pressure/flux linear response of the aqueduct. We also evaluate the complex impedance $Z^k = 1/Y^k$ and find for all patients that $\mathrm{Im}(Z^k) > 0$. Thus, the electric model of the aqueduct is a self-inductance with $Z^k = R^k + iL^k\ \omega^k$. Using the first three mode truncation leads to the total

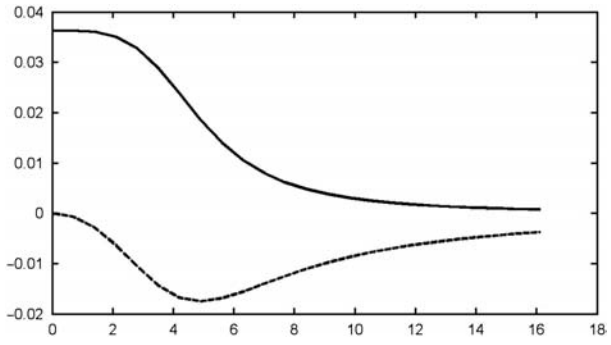

Figure 1. Complex admittance Y: real part C (top) and imaginary S (bottom) versus Womersley.

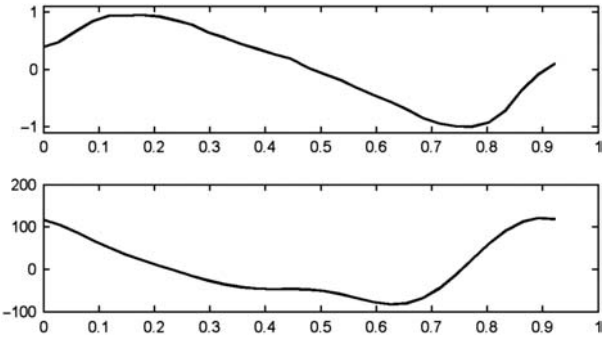

Figure 2. Reconstructed pressure drop (bottom) and experimental MRI flux (top) over a cardiac cycle.

pressure drop reconstruction for the aqueduct (see Figure 2)

$$\Delta P = R^0 Q_s + \sum_{k=1}^{3} \mathrm{Re}\,(Z^k Q_u^k e^{i\omega^k t})$$

4. Conclusions

Our results show that the leading order contribution comes from the three first oscillatory modes. As the Womersley number is non zero, the resulting admittance is complex. Futhermore, our evaluation shows that the resistance part R^k does not predominate over the inductance part L^k. In conclusion, we propose a simple and very fast method to evaluate (quasi-analytically) the aqueduct admittance from patient based MRI anatomical images and Cine aquisitions. Furthermore, we can reconstruct the total pressure drop across the aqueduct. This method can be used in the future to access systematic patient investigation and provide interesting non-invasive parameters for therapeutical studies.

References

Fin L, Grebe R. 2003. Three-dimensional modeling of the cerebrospinal fluid dynamics and brain interactions in the aqueduct of Sylvius. Computers methods in biomechanics and biomedical engineering. 6:163–170.

Sweetman B, Xenos M, Zitella L, Linninger A. 2011. Three-dimensional computational prediction of cerebral fluid flow in the human brain. Computers in biology and medecine. 41:67–75.

Tain R, Alperin N. 2009. Compliance effect on amplitude and phase of cranio-spinal CSF flow measured by MRI. Bioinformatics and biomedical engineering. 3:1–4.